Zheng, Ge, Yan, Yong, Wang, Lijuan, Hu, Yonghui and Zeng, Xingxing (2024) ***Concurrent measurement of the size distribution and velocity of pneumatically conveyed biomass solids using acoustic emission and electrostatic sensors.*** **IEEE Transactions on Instrumentation and Measurement, 73 . ISSN 0018-9456.**

Concurrent Measurement of The Size Distribution and Velocity of Pneumatically Conveyed Biomass Solids Using Acoustic Emission and Electrostatic Sensors

Ge Zheng, Yong Yan, *Fellow, IEEE*, Lijuan Wang*, *Senior Member, IEEE*, Yonghui Hu, *Senior Member, IEEE*, and Xingxing Zeng

***Abstract*—In biomass fired power plants accurate measurement of the size distribution and velocity of biomass solids in pneumatic conveying pipelines feeding the burners is essential to maintain high combustion efficiency and reduce pollutant emissions. In this article, a new method for the size distribution and velocity concurrent measurement of biomass solids through acoustic emission (AE) detection and electrostatic sensing is proposed. When an AE waveguide protrudes into a biomass fuel pipe, an AE signal is generated due to the impact of biomass on the waveguide. In consideration of the inelastic and irregular characteristics of biomass fuels, the Stronge model is introduced to describe the inelastic impact process. The relationship between the statistical value of equivalent impact size and the shape characteristics of irregular shaped solids is analyzed. Meanwhile, the velocity of biomass fuel is determined by processing the signals from arc-shaped electrostatic sensor arrays. The fusion of the peak amplitude of the AE signal and biomass velocity allows the measurement of biomass size distribution. Experimental tests with crushed wheat straw, sawdust and corncob were conducted on a laboratory-scale pneumatic conveying test rig to assess the effectiveness of the size distribution measurement technique. The experimental results demonstrate that the measured biomass velocity varies with the air velocity and the transport capacity of the conveying air to biomass solids depends on factors such as shape and size distributions of biomass fuels. The relative error of the measured mean biomass size is within ± 6.45% under all test conditions with a standard deviation within 2.15%.**

***Index Terms*—Pneumatic conveying, biomass, size distribution, acoustic emission (AE).**

I. Introduction

BIOMASS is an energy source with zero carbon emissions throughout its life cycle and its resource supply is stable, which makes biomass fired power generation a low-carbon, efficient and highly flexible way of producing electricity. In recent years the installed capacity of biomass power plants has be increasing continuously [1, 2]. In biomass power plants, biomass materials such as sawdust, straw and corncob are crushed and pneumatically conveyed to the boiler for combustion. The flow characteristic parameters of biomass solids, such as velocity and size distribution, have an important impact on the safety, efficiency and emissions of the combustion process [3, 4].

However, gas-solid two-phase flow is complex in nature while the concentration of pulverized fuel in a pneumatic conveying pipeline is dilute [5]. The accurate online measurement of the flow parameters of pneumatically conveyed solids is a technical problem that has plagued academia and industry for many years [5-7]. A lot of research work has been carried out on the flow of powdered fuel [8-11]. Due to the inherent limitations of the existing measurement technology, such as complex system design, high implementation costs and poor adaptability to harsh environmental conditions, there is still a lack of reliable detection systems that can monitor the flexible and variable solid flow in the power plant for a long time [12].

For the measurement of gas-solid two-phase flow parameters, especially particle size and velocity, there are laser technology [13, 14], digital image technology [15, 16], ultrasonic technology [17, 18], electrical technology [19, 20] and so on. The optical techniques, such as laser and image technology, can directly observe the shape information of solids, so they have significant advantages in off-line measurement of irregular solids size. However, in the online measurement environment of the industrial field, the tiny solid in the pneumatic conveying pipeline are easily adsorbed on the optical window. Moreover the optical components are also easily worn by the flowing solids in the long-term use. The advantage of the electrical technique is that the structure of the sensor is simple and the cost of manufacturing and maintenance is low. However, the capacitance and electrostatic value are easily affected by environmental factors and the water content of the solids. The

Manuscript received Month xx, 20xx; revised Month xx, 20xx; accepted Month xx, 20xx.. The Associate Editor coordinating the review process was xx. (*Corresponding author: Lijuan Wang*)

Ge Zheng is with the Distribution Technology Center, China Electric Power Research Institute, Beijing 100192. Yong Yan is with Hangzhou International Innovation Institute, Beihang University, Hangzhou 311115, China. Lijuan Wang is with School of Engineering, University of Kent, Canterbury, Kent CT2 7NT, U.K(Corresponding author email: l.wang@kent.ac.uk). Yonghui Hu and Xingxing Zeng are with School of Control and Computer Engineering, North China Electric Power University, Beijing 102206, China.

ultrasonic technique is not suitable for the measurement of non-uniform solid flow. Meanwhile, the measurement results are easily affected by the rapid attenuation of sound waves and the excessive noise caused by the collision between solids.

Recently, AE detection technology is regarded as a promising method for on-line measurement of solid size. The AE detection technique relies on the analysis of the elastic wave generated by the impacts between solids and obstacles to obtain the movement information of solids. It is highly sensitive, simple in structure, insensitive to changes in environmental conditions such as temperature and humidity, and can adapt to harsh industrial environments. AE signal contains lots of information about solid flow, which has a direct physical relationship with the flow parameters, but it is difficult to extract a single effective parameter. According to Hertz impact theory, Boschetto *et al.* [21] recognized solids with different size by using the AE peak voltage generated by impacts between solids and a flat plate. Droubi *et al.* [22] explored the AE signal energy during impacts between solids and a carbon steel plate. The experiment results demonstrate that the AE signal energy is proportional to the cube of solid size, while the AE signal energy generated by multi-solid impacts is cumulative to that generated by single-solid impact. Hansold *et al.* [23] established a relationship between power spectral density characteristics of AE signal and solid size. However, this model only allows for qualitative measurement. Coghill [24] designed a AE-based system that allows the AE device to be inserted deep into the pipe for solid size measurement based on contact time. However, it was found from experiments that when the air velocity in the pipe is 20~30 m/s, the estimation of contact time has a large deviation, which leads to the invalidation of the measurement method. Zheng *et al.* [25] conducted the measurement of the size distribution of pneumatically conveyed solids using AE and electrostatic sensors based on Hertz impact theory. The measurement mainly aimed at silica sand solids with relatively regular shape and hard material. Gao *et al.* [26] inserted a V-shaped waveguide into the pipe to generate AE signals. Based on Hertz impact theory, the mathematical relationship between the AE peak voltage and solids size, velocity was derived. However, the size measurement model is based on the assumption that biomass solids are perfectly elastic spheres. The solids velocity was replaced by the air velocity, resulting in the velocity measurement error. The current research has preliminarily verified the effectiveness of solids size measurement based on AE detection technique. However, most of the work is still based on experimental studies to collect AE signals and then attempts are made to establish relationship between AE signal characteristics and solids size. The size measurement of solids is mainly based on Hertz impact theory and the idealized assumption of spherical solid impacts, and lack of the consideration of solids velocity information.

Electrostatic sensing method has been widely studied in the measurement of velocity, concentration and mass flow rate of gas-solids two-phase flow [27-29]. The electrostatic sensing method establishes a relationship with solid flow parameters by detecting the strength of the electric field around charged solids [27]. It has the advantages of low manufacturing and maintenance costs, simple structure, passive measurement and wide sensing range. The main disadvantage of the electrostatic sensing method is that the charge on solids depends on a series of factors. In case of variations in the transport environment of solids flow, such as changes in temperature and humidity, parameter calibration is required for the models that depend on electrostatic signal amplitude [30]. In contrast, cross-correlation velocity and relative concentration measurements utilize the relative relationship of multiple electrostatic signals in a similar environment, making the measurements more reliable. Furthermore, the solids velocity measured from electrostatic sensors can provide information supplement for extracting solid size parameters from AE signals.

Whereas most of biomass solids are significantly different from regular solids. Biomass solids are usually flexible and extremely irregular in shape. The traditional elastic impact model cannot describe the impact process of biomass solids. In addition, biomass solids have larger size and wider distribution range. These properties make the flow characteristics of gas-solid two-phase flows generated by biomass solids more complex and variable, increasing the uncertainty and difficulty of flow measurement.

In this article, an innovative method for size distribution and velocity measurement of biomass solids using AE and electrostatic sensors is proposed. The absolute and direct relationship between the AE signal and the flow parameters can compensate for the shortcomings of the electrostatic sensing method, while the relative information on the solids fluctuations provided by the electrostatic signal can complement the information for extracting the flow parameters from the AE signal. Meanwhile, in consideration of inelastic and irregular characteristics of biomass solids, the biomass solid size distribution model is established. When the AE waveguide is extended into the solids flow, the collision of solids with the waveguide generates AE signal, the peak voltage of which contains information including the size and velocity of impacting solids. Firstly, the inelastic impact theory is introduced to describe the inelastic collision process for the biomass solids. Meanwhile, the relationship between the statistical value of solids size and the shape characteristics of irregular solids is analyzed. Secondly, the velocity information of biomass solids is obtained through arc-shaped electrostatic sensor arrays using multiple cross-correlation algorithm. Thirdly, the measurement method of biomass size distribution is established in combination with the solid velocity and AE peak voltage. Finally, in the laboratory scale pneumatic conveying system, the commonly used solids of biomass power plants were utilized for experiments to analyze the transport capacity of conveying air to different biomass solids, as well as the reliability and accuracy of size distribution measurement under different test conditions. With the advantages of high sensitivity, low manufacturing and maintenance costs, and suitability for operation in harsh industrial environments, the instrumentation system combining AE and electrostatic sensors provides a new technical solution to the concurrent measurement of the size distribution and velocity of pneumatically conveyed biomass solids.

The article is organized as follows: Section II describes the measurement methodology of the distribution and velocity of pneumatically conveyed biomass solids is proposed. In Section III, the instrument system and experimental setup are introduced, and then the measured data are statistically analyzed. Section IV gives conclusions and prospect of the work presented.

II. METHODOLOGY

A. Overall strategy

The AE signal generated by impact of a biomass solid is closely related to the impulsive force that the biomass solid imposes on the AE waveguide. The contact force depends on biomass characteristics, especially solids size and velocity. Meanwhile, the charged biomass solids flowing through the electrodes arranged upstream and downstream of the pipeline will generate similar electrostatic signals. Combined with the cross-correlation signal processing method, the solids velocity information can be obtained.

Most of biomass solids are easily deformed and extremely irregular in shape. In addition, most of biomass solids have large size and wide distribution range. Due to nature characteristics of biomass solids, biomass solid flow is more complex and dynamic than conventional gas-solid two-phase flow, which increases the uncertainty and difficulty of flow measurement. Fig. 1 shows the key stages of the biomass size and velocity measurement strategy. Firstly, an AE waveguide and electrostatic sensor arrays are respectively used to acquire AE signals generated by continuous impacts of biomass solids and electrostatic signals generated by charged solids flowing through the electrodes. Secondly, through peak detection algorithm and Rosin-Rammler modification, the AE peak voltage generated by the impact of an individual biomass solids is extracted from the collected AE signal. Meanwhile, the local solids velocities are obtained through multi-channel cross-correlation of collected electrostatic signals. Thirdly, with consideration of the irregular shape of biomass and plastic collision, the impact velocity fusing from local solid velocities and the modified peak distribution are substituted into the biomass solid impact model, and then the size distribution measurement of biomass flow is achieved. Meanwhile, the cross-sectional velocity of biomass flow is obtained by fusing the local solids velocity.

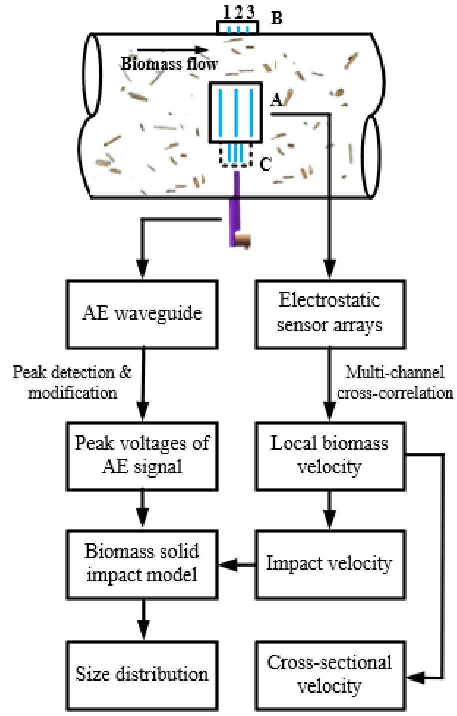

Fig. 1. Measurement strategy of the biomass sizing system.

B. Biomass impact modelling

Biomass materials are prone to irreversible deformation when subjected to external forces [31, 32]. Therefore, the Hertz collision theory based on the assumption of perfectly elastic collisions is not suitable for biomass size measurement, whereas plastic deformation is not negligible in the measurement. Moreover, biomass solids are extremely irregular in shape, so the impact of irregularity on the stability and repeatability of measurement results needs to be considered. When comparing the measurement results with the reference solids size, the relationship between the equivalent sizes measured by different methods should also be considered.

By quantifying the ratio between the collision duration and the period of the natural mode shape of the colliding object, Stronge [33] divided the compression process after the impact on the plate into three stages, namely a fully elastic compression stage, an elastic-plastic mixed compression stage and a fully plastic compression stage.

Assuming that the contact area of the AE waveguide is a plane, based on the Stronge model and Newton's second law, the contact force changes during compression can be expressed as follows. At the fully elastic compression stage, the contact force is consistent with that described by the Hertz impact theory, which can be obtained as

$$F_c(t) = m\ddot{s}(t) = -Ks(t)^{\frac{3}{2}} \tag{1}$$

where m is the mass of the solid, $s(t)$ is the deformation displacement, and K is a constant that can be defined as

$$K = \frac{4}{3}\sqrt{\frac{d}{2}}\left(\frac{1-\mu_1^2}{E_1} + \frac{1-\mu_2^2}{E_2}\right)^{-1} \tag{2}$$

where μ_1 and μ_2 are the Poisson's ratio of the solid and waveguide, respectively, E_1 and E_2 are the Young's modulus of the solid and waveguide, respectively, and d is the solid diameter. The critical deformation displacement s_c at this stage is

$$s_c = \frac{9}{8}\left(\frac{\pi b_1 Y}{K}\right)^2 d^2 \tag{3}$$

where Y is the yield stress of the solid, which is related to its diameter, i.e., $Y \propto d^{-\frac{1}{2}}$ [34], and b_1 is the proportionality constant between the critical stress and the yield stress at the fully elastic compression stage, usually taking a value of 1.1 [35].

At the elastic-plastic mixed compression stage, the contact force is expressed as

$$F_c(t) = m\ddot{s}(t) = -F_{cp}\left[\frac{2s(t)}{s_c} - 1\right]\left[1 + \frac{1}{3.3}\ln\left(\frac{2s(t)}{s_c} - 1\right)\right] \tag{4}$$

where F_{cp} is the critical value of the contact force when changing from the fully elastic compression stage to the elastic-plastic mixed compression stage. The critical deformation displacement s_c at this stage is

$$s_{cp} = 0.5 s_c\left[e^{2.25(b_2 - b_1)^2} + 1\right] \tag{5}$$

where b_2 is the proportionality constant between the critical stress and the yield stress at the elastic-plastic mixed compression stage, usually taking a value of 2.8 [35].

When the compression deformation is greater than s_{cp}, the compression enters the fully plastic compression stage. At this stage, the contact force is

$$F_c(t) = m\ddot{s}(t) = -F_{cp}\frac{b_2}{b_1}\left[\frac{2s(t)}{s_{cp}} - 1\right] \tag{6}$$

Spherical wheat straw, sawdust and corncob solids with a diameter of 1 mm were set to collide with a zirconia ceramic plate at a velocity of 20 m/s, respectively. Fig. 2 plots the impact contact force versus time. As shown in Fig. 2, contact forces of biomass increase with time, reach a peak and then decrease gradually. Contact force curves of wheat straw and sawdust are similar, whereas the contact force of corncob solids is smaller and the collision duration is longer. Assuming that the propagation process of the elastic wave in the waveguide and the response function of the AE sensor are linear and time-invariant, the peak value of the AE signal generated by an individual collision is proportional to the maximum contact force. With the known peak value of AE signal and collision velocity, the solids size can be obtained.

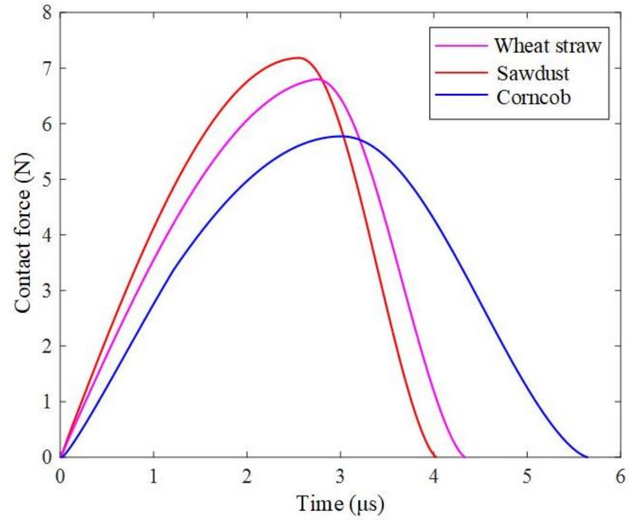

Fig. 2. Contact forces during the impacts of three biomass solids with zirconia plate.

The size of irregular solids measured by any solid sizing instrument is the equivalent value. Therefore, for the size measurement of irregular solids, the repeatability of the measurement results is a key performance indicator of the measurement system [36, 37].

The solids size measurement through AE detection is based on the impact theory, so the measured size is the equivalent impact diameter. Fig. 3 is illustration of spherical and non-spherical solids impacting on a flat plate. Based on the impulse equation and Coulomb friction law, Sommerfeld [38] simulated multiple collisions of a variety of non-spherical solids with the same equivalent projected area diameter. It is found that the average value of the impact radius R_c of a non-spherical solid varies little with the impact angle α under multiple collisions. Moreover, the impact radius of non-spherical solids with the same equivalent projected area but different shapes increases linearly with the decrease of the solid's width-to-length ratio in the case of a non-minimum impact angle, i.e.,

$$d_c = \frac{d_{sa} - L}{r_{lw}} + L \tag{7}$$

where d_c is the average value of the solid impact diameter, d_{sa} is the equivalent projected area diameter which can be measured through solid imaging, r_{lw} is the solid aspect ratio, and L is the solid length. In a large collection of solids, there are many collision events generated by solids of similar shape and size. The statistical value of solids impact diameter is stable to the measured solids and is closely related to the actual shape and size. Therefore, the measured size distribution of irregular solids based on impact theory can reflect the actual size distribution of irregular solids.

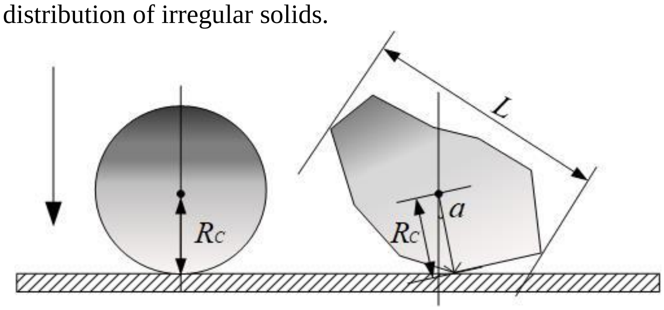

Fig. 3. Illustration of spherical and non-spherical solids impact on a flat plate.

C. Peak detection and modification

The AE signal generated by a single collision event exhibits a single peak shape followed by a damped oscillation wave. To obtain the size distribution of biomass flow by the biomass solid impact model, the signal peak of individual collisions should be identified.

A peak detection algorithm [39] based on the local energy is used to determine the AE signal peaks. For a sequence of AE signal (V), the local energy of the kth sampling point is defined as

$$E_k = \frac{1}{N}\sum_{i=k-\frac{N}{2}}^{\frac{N}{2}-1}(V)^2 \tag{8}$$

where N is the length of the sliding window. In this algorithm, firstly, the local energy of each sampling point on the collected AE signal is calculated. Secondly, the energy envelope is smoothed by means of mean filtering to eliminate false peaks. At the same time, peak points higher than the surrounding four points is found on the smoothed local energy envelope. Thirdly, a threshold is set to eliminate false peak points due to ambient noise. Finally, the signal peaks/valleys are determined in the original AE signal according to the corresponding energy peak position.

However, in practical situations, due to simultaneous impacts of multiple solids and the airflow noise, some of the detected AE peaks are overlapped and AE pluses generated by small solids impacts are drowned in noise and the setting threshold. So the detected peak distribution usually deviates from the expected distribution, especially at segments of the largest and smallest peaks. Consequently, the measurement accuracy of the solids size distribution will be reduced. The Rosin-Rammler model is usually used to characterize the solids size distribution of powders obtained by grinding, milling and crushing, and good correlations have been verified experimentally [40, 41]. The general expression of the Rosin-Rammler model is as follow:

$$F(x) = 1 - e^{-\left(\frac{x}{x_{50}}\right)^m} \tag{9}$$

where $F(x)$ is the distribution function, x is a random variable, x_{50} is the median of x, and m is the distribution modulus to determine the distribution range. x_{50} and m are parameters describing the properties of the distribution. The calibration of the Rosin-Rammler model is performed on the peak segments which are less affected by the signal overlapping and noise. According to the calibration results, m and x_{50} can be determined. The Rosin-Rammler prediction is then applied to the entire distribution to modify the peak segments generated from larger and smaller solids, thereby reducing the peak distribution deviation due to the impact overlapping and airflow noise.

D. Principle of biomass velocity measurement

As the biomass flow through the upstream and downstream electrodes, electrostatic signals with similar waveforms are generated through electrostatic induction. The time delay of the biomass passing through the two electrodes, that is, the transit time, is obtained by performing correlation analysis on the electrostatic signals. The velocity measurement of biomass flow is achieved with the obtained transit time and known electrode spacing [13].

Each pair of electrodes in the electrostatic sensor array (Fig. 1) is used to measure a cross-correlation velocity v_{ij}

$$v_{ij} = \frac{L_{ij}}{\tau_{ij}} \tag{10}$$

where i and j represent electrodes 1, 2 or 3, and L_{ij} is the axial space between the upstream electrode i and the downstream electrode j. According to the cross-correlation function of the electrostatic signals output by electrodes i and j, the transit time (τ_{ij}) is determined from the location of the dominant peak of the cross-correlation coefficient (ρ_{ij}). The weighted average solids velocity from the electrostatic sensor arrays A, B and C, namely v_1, v_2 and v_3, is determined from the three individual cross-correlation velocities

$$v_z = \frac{\rho_{12}v_{12} + \rho_{23}v_{23} + \rho_{13}v_{13}}{\rho_{12} + \rho_{23} + \rho_{13}} \tag{11}$$

where z=1, 2 or 3.

The solids phase velocity ($v_s(t)$) in the gas-solids two-phase flow is defined as the instantaneous average solids velocity in the pipe cross-section, i.e. [5]

$$v_s(t) = \frac{\int\int v(x,y,t)\beta(x,y,t)dxdy}{\int\int \beta(x,y,t)dxdy} \tag{12}$$

where $v(x, y, t)$ is the axial velocity of the solid at the position (x, y) over the pipe cross section at time t, and $\beta(x, y, t)$ is the proportion of the solid in the pipe section. Although biomass solids are non-uniform distributed over the pipe cross section, other transport conditions such as temperature and humidity in the pipe are similar and the solids are in dilute suspension flow. So the volume concentration ratio of local solids can be expressed as the root mean square ratio of the electrostatic signal (A_{rms}) [5, 29]. Therefore, for the biomass flow with a non-negligible inhomogeneous solids distribution, the cross-sectional solids velocity can be calculated as

$$\bar{v} = \frac{\sum_{z=1}^{3} v_z A_{rms,y}}{\sum_{z=1}^{3} A_{rms,y}} \tag{13}$$

Since the electrostatic sensor arrays A and C are symmetrically mounted near the waveguide, fusing the solid velocities from the arrays A and C can approximate the solid impact velocity to assist in the analysis of the AE signal, i.e.

$$v_{AE} = \frac{v_1 A_{rms,1} + v_2 A_{rms,2}}{A_{rms,1} + A_{rms,2}} \tag{14}$$

III. Experimental Results and Discussion

A. Experimental setup and test conditions

In order to evaluate the effectiveness of the proposed method, experimental tests were undertaken on a laboratory-scale pneumatic conveying rig, as shown in Fig. 4. An industrial suction system with adjustable power is used to generate stable air flow with different velocities. A vibratory feeder supplies biomass from a hopper at a controlled mass flow rate. The inner diameter of the pneumatic conveying pipe is 72 mm. The sensing head, mounted on the vertical pipeline at a distance of 1100 mm from the upstream elbow, is composed of an AE waveguide and electrostatic sensor arrays. As shown in Fig.5, in order to obtain effective signals and reduce overlapping impact events, a semi-cylindrical AE waveguide, with an intrusion area of 70 mm^2 flat surface facing the biomass flow, is used as an impact target to generate the AE signal. Rubber bushings are used to tightly wrap the middle section of the waveguide to prevent pipe vibration from affecting the signal. The AE sensor is attached to the outer end of the waveguide. Three sets of electrostatic sensor arrays are evenly embedded in the tube wall at an angular interval of 120° to measure the biomass velocity. In order to prevent the turbulence interference caused by the charged solids flowing by the AE waveguide at the upstream and downstream, the sensor arrays A and C are installed near the two sides of the waveguide. Each set of sensor array consists of three identical electrodes with an area of 180 mm^2 per electrode and the distance between the adjacent electrodes is 20 mm. A shielding stainless steel cover was used to isolate the entire electrostatic sensor arrays from the external environment to prevent electromagnetic interference.

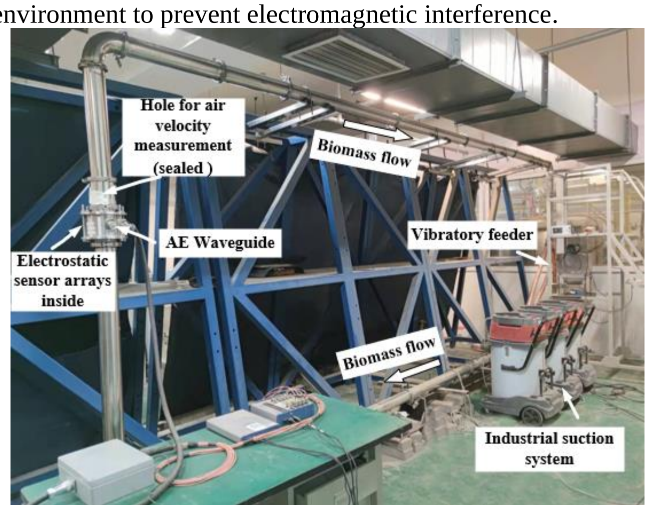

(a)

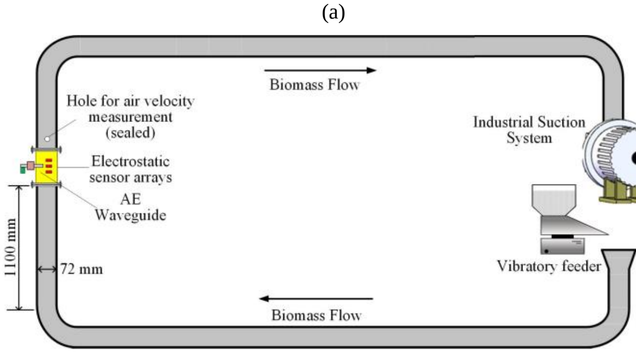

(b)

Fig. 4. Biomass flow test rig. (a) Photo of the test rig. (b) Schematic of the test rig.

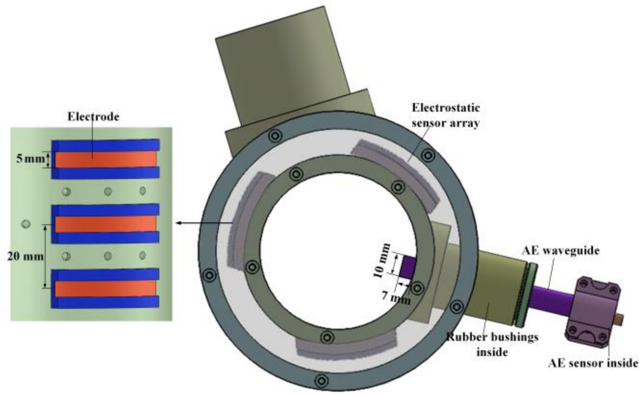

Fig. 5. Design of the sensing head.

Wheat straw, sawdust and corncob are common biomass fuels in biomass power plants [1, 4]. In this study, the three types of biomasses were used as test solids as they have different physical properties. Fig. 6 shows the images of the three biomass fuels. As can be seen, the shapes of biomass are different, while most of them are in square shapes and elongated. Due to the large size and highly irregular shape of the biomass fuels, the measurement results of image method are usually used as the reference solid size. An established biomass imaging equipment composed of HP-G4010 flatbed scanner and BioMscan software developed by Robert Carter of the University of Kent[42] was used to obtain the reference size distribution and shape (aspect ratio) distribution. Since the biomass solids are not spherical, the equivalent size is used in this study, where the cross-sectional area of a solid is equivalent to a circle, the diameter of which is regarded the size of the solid. Meanwhile, the longest diameter across the solid is regarded as the length of the solid. The imaging results of wheat straw, sawdust and corncob are summarized in Table I with their equivalent size and length distributions are shown in Fig. 7. Among them, the wheat straw has the highest irregularity and the largest length, which is in the shape of slender strip with a mean aspect ratio of 2.78, The sawdust is in the form of bars and squares and the largest of the three in terms of mean size. The corncob is the smallest in size, but is closest to the spherical shape with a mean aspect ratio of 1.72. The corncob is the lightest among the three in terms of true density.

(a)

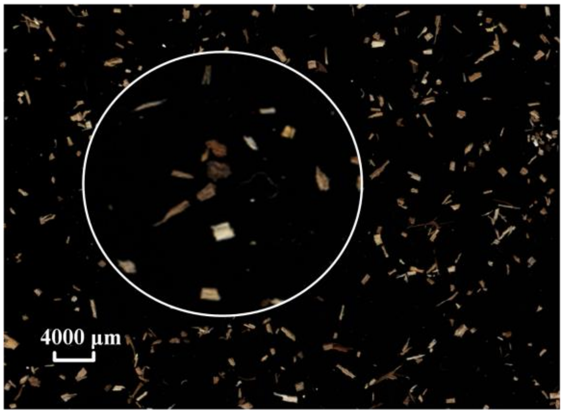

(b)

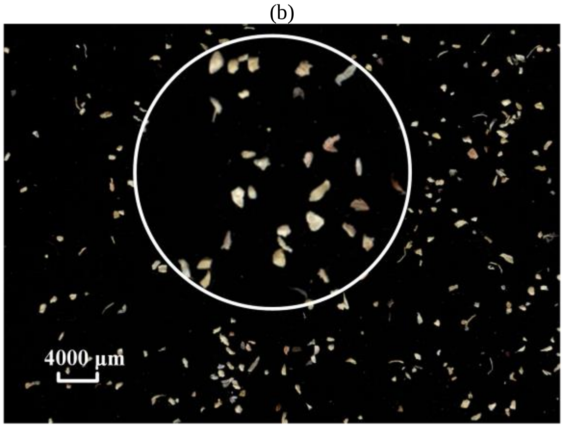

(c)

Fig. 6. Typical images of biomass fuels. (a) Wheat straw. (b) Sawdust. (c) Corncob.

Table I Characteristic Parameters of the Biomass fuels

Biomass type	Mean size (mm)	Mean length (mm)	Mean length-width ratio	True density (kg/m^3)
Wheat straw	1.32	2.70	2.78	1180
Sawdust	1.38	2.40	2.27	1120
Corncob	0.90	1.58	1.72	1030

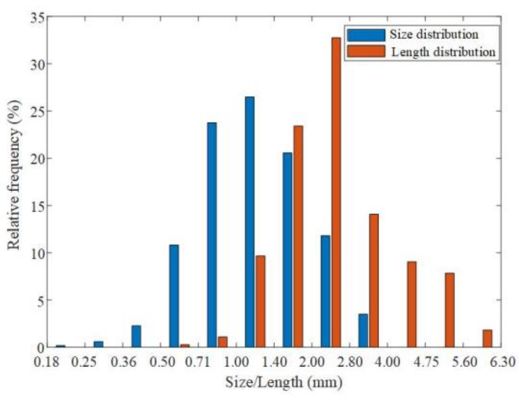

(a)

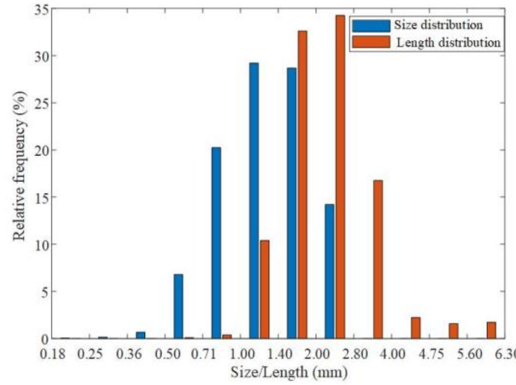

(b)

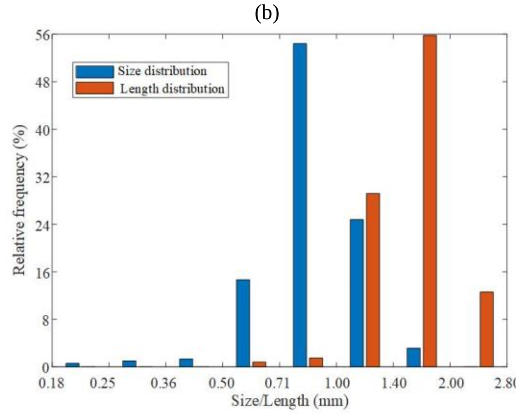

(c)

Fig. 7. Size and length distributions of the test solids measured from Biomass imaging system. (a) Wheat straw. (b) Sawdust. (c) Corncob.

For each type of biomass, experiments were conducted under 20 test conditions, as summarized in Table II. All experiments were carried out under an ambient temperature of 17~20°C and relative humidity of 45~49%. In order to avoid a drop in air velocity due to the prolonged operation of the industrial suction system, a differential-pressure anemometer (MP210, KIMO) was used to calibrate the air velocity and the power of the corresponding suction system through the air velocity measuring hole near the sensing head. The calibration process was repeated for 5 times, thus the uncertainty was ±1%. After calibration, the air velocity measuring hole shall be sealed with blu-butyl rubber. The mass flow rate is determined by weighing the feeding amount of the vibratory feeder within one minute to determine the corresponding amplitude voltage. The calibration experiment was repeated for 5 times, thus the uncertainty is ±3%. In consideration of the instability of biomass flow, the AE signal was acquired over a period of 30 s with a sampling rate of 2 MHz under each test condition. Meanwhile, the signals from the electrostatic sensor arrays were sampled at 20 kHz.

Table II Experimental Conditions

Mass flow rate (kg/h)	Air velocity（m/s）				
	V_1=24	V_2=28	V_3=32	V_4=36	V_5=40
M_1=9.0	V_1M_1	V_2M_1	V_3M_1	V_4M_1	V_5M_1
M_2=14.4	V_1M_2	V_2M_2	V_3M_2	V_4M_2	V_5M_2
M_3=19.8	V_1M_3	V_2M_3	V_3M_3	V_4M_3	V_5M_3
M_4=25.2	V_1M_4	V_2M_4	V_3M_4	V_4M_4	V_5M_4

B. Biomass velocity measurement

Fig. 8 shows the typical signal waveforms from electrostatic sensor array A. It is evident that the signals from the three electrodes have a similar pattern with a certain time delay between them. It is unsurprising to encounter minor variations among the three electrostatic signals, as they stem from diverse contributing factors. These include fluctuations in the solid velocity pattern traversing the pipe's cross-sectional area, particle attachment at the electrode sites, mechanical allowances during the manufacturing process of electrodes, insulators, and the sensing head assembly, and inconsistencies within the three-channel signal conditioning electronics. As can be seen in Fig. 8, the dominant peak of the cross-correlation coefficients are 0.61(ρ_{12}), 0.48(ρ_{23}), 0.30(ρ_{13}), respectively. The transit time determined from the location of the dominant peak of the cross-correlation coefficients are 0.92 ms(τ_{12}), 0.96 ms(τ_{23}), 1.84 ms(τ_{13}), respectively. Therefore, the local solid velocity can be obtained as 21.43 m/s by formulas (10) and (11).

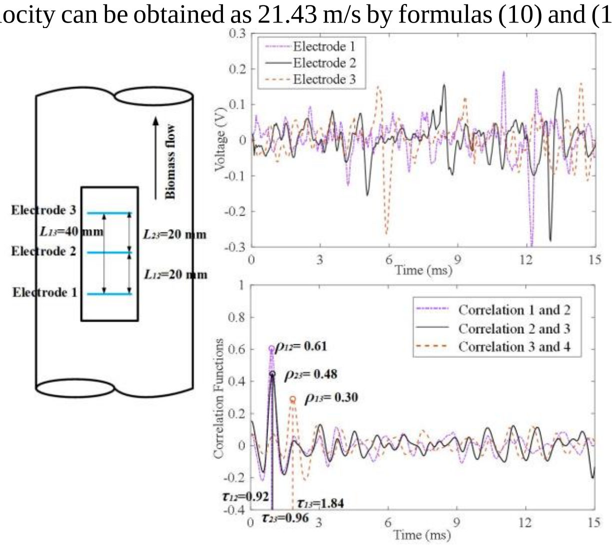

Fig.8. Typical signal waveforms and corresponding correlation functions from electrostatic sensor array A.

Fig. 9 plots the measured velocities of the biomass fuels at a mass flow rate of 9.0 kg/h. Each data point is the average of 30 correlation velocities of biomass measured over a 1 second period. The 'error' bars in Fig. 9 represents the standard deviation of the measured velocities. It is clear that the velocity of wheat straw fluctuates significantly more than those of sawdust and corncob, while corncob velocity is the most stable. Therefore, for the same air velocity, biomass with a higher degree of irregularity and larger size, such as wheat straw and sawdust, has greater velocity fluctuations than the relatively regular shaped biomass such as corncob. Moreover, Fig. 9 indicates the local velocities measured through the three sensor arrays do not deviate much without a clear distribution pattern. The deviations in the measured velocities are mainly due to natural fluctuations of biomass solids. The impact velocity for solids size measurement is determined by fusing the two local velocities measured from the sensor arrays A and C, which are close to AE waveguide, as shown in Fig. 5. The inhomogeneity of the gas-solid two-phase flow results in the difference between the local velocity measured from sensor array B and the impact velocity synthesized from the signals of the sensor arrays A and C.

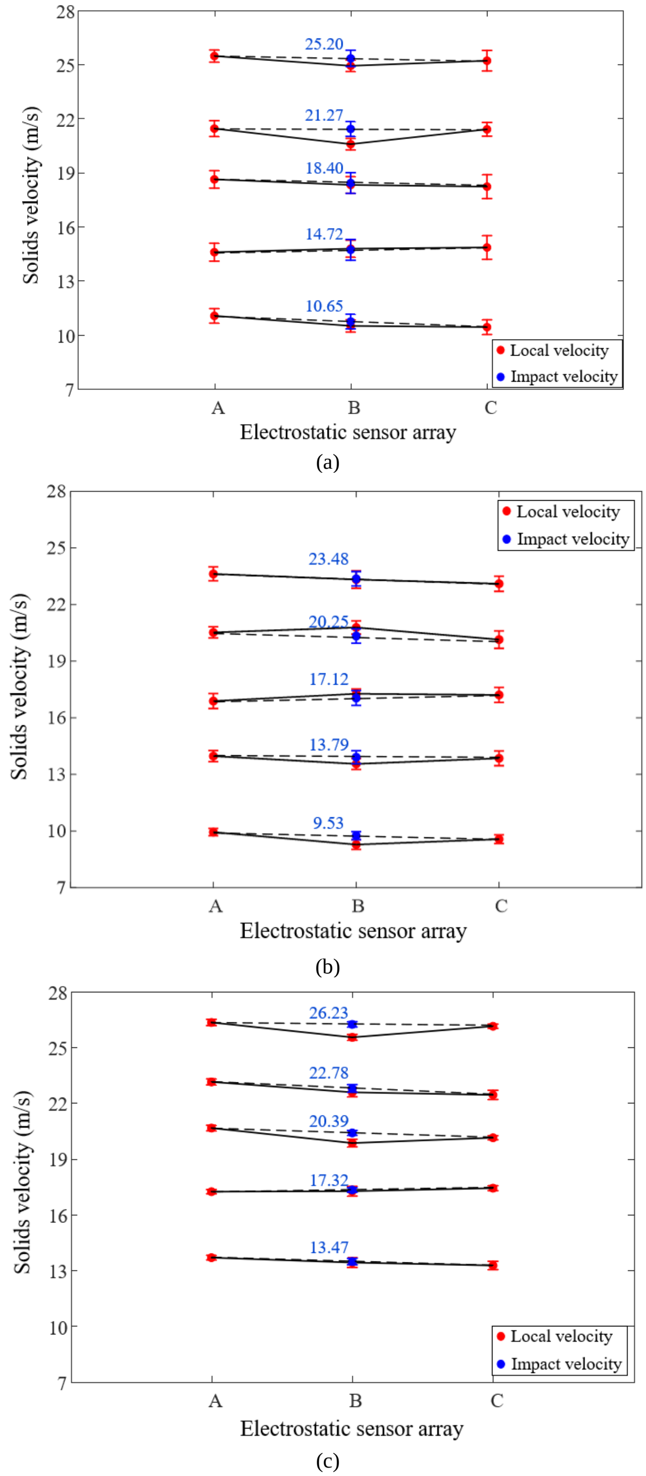

Fig. 9. Measured velocities of biomass fuel. (a) Wheat straw. (b) Sawdust. (c) Corncob.

Fig. 10 illustrates a direct comparison between the measured cross-sectional solids velocity and the air velocity for the three biomass solids. As can be seen, the solids velocity measured from the sensor arrays follows the same trend as the air velocity. For the same air velocity, however, sawdust was transported at the slowest speed whilst corncob the fastest. The mean slip velocity between biomass (sawdust, wheat straw, corncob) and conveying air is 15.16 m/s, 13.95 m/s and 12.07 m/s, respectively. The slip velocity is almost independent of the air velocity and depends mainly on the shape and size of biomass

[43]. As expected, corncob as the smallest and lightest biomass has the smallest slip velocity. Sawdust and wheat straw are similar in average solid size and density (Table I). Wheat straw has a slightly lower slip velocity than sawdust because most of its solids are in the shape of slender strips. Such results suggest that size and shape of biomass fuels have to considered in the design and operation of pneumatic conveying systems at biomass power plants. In order to achieve the desired conveying velocity and prevent solids stratification and deposition in the pipe network, the air velocity should be adjusted for different biomass fuels.

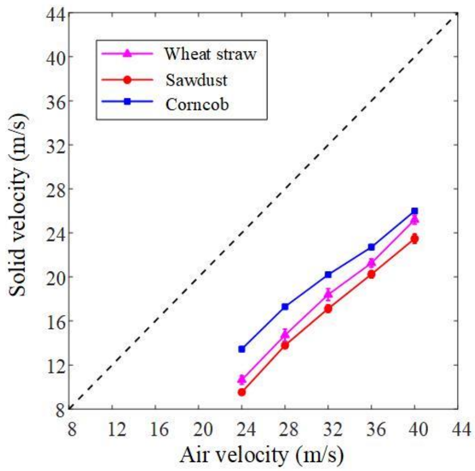

Fig.10. Comparison between biomass and air velocities for the three biomass fuels.

C. Biomass size distribution measurement

The typical AE signals and their power spctrums from the three biomass fuels at an air velocity of 32 m/s and a mass flow rate of 9.0 kg/h are shown in Fig. 11. As can be seen, the power spectra of the AE signals from the three biomass fuels are mainly concentrated in 0-200 kHz. Most impact events can be distinguished in the signals, while the AE signal peaks are different under the impact of different sized solids.

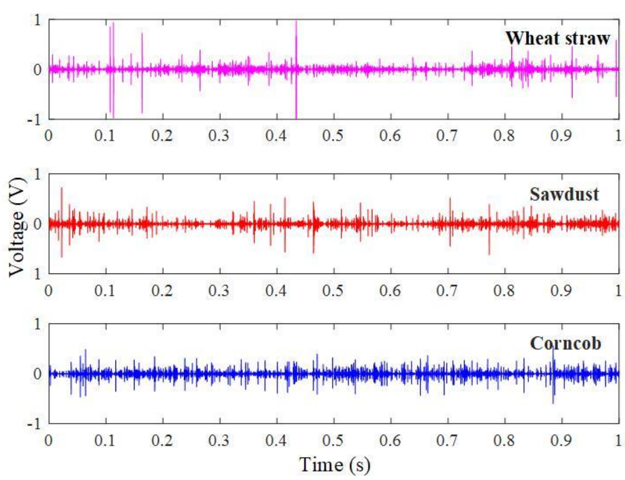

(a)

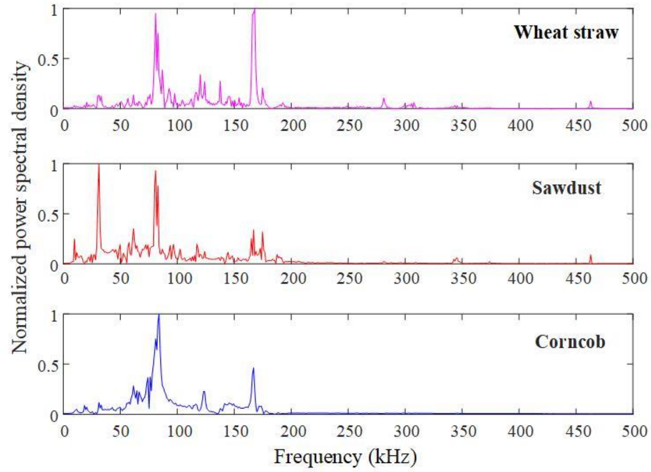

(b)

Fig.11. Typical AE signals and their corresponding power spectra for the three biomass fuels. (a) AE signal waveforms. (b) Normalized power spectrum.

As shown in Figs 12, 13 and 14, the measured size distribution of wheat straw is the largest, followed by sawdust and corncob the smallest. The equivalent size distribution of sawdust is close to that of wheat straw, while that of corncob is relatively concentrated. The overall measured results are consistent with the trends in the size distribution measured from the imaging method (Table I). Since wheat straw has the highest irregularity and largest in size, theoretically the same wheat straw is likely to result in different impact size in different impact events. As shown in Fig. 12, under nine different test conditions, the standard deviations of the size distribution of wheat straw are all less than 1.88%. In the set of impact events generated by solids on the AE waveguide in 30 s, there are multiple impact events of solids with similar shapes and sizes. While the measured equivalent size distribution of biomass fuels is the statistically averaged, the result can represent the actual size of wheat straw. As shown in Figs 13 and 14, the standard deviations of size distributions of sawdust and corncob are less than 1.57% and 2.15%, respectively. When the air velocity is small or the mass flow rate is large, some solids will collide with the waveguide at the same time. The overlapping impact solids are misrecognized as large size solids, resulting in the deviation of the center of gravity of the measured equivalent size distribution, so some of standard deviation shows a bimodal distribution. If the overlapping impact problem is further exacerbated, the contact area of the AE waveguide needs to be reduced. Overall, for the three biomass fuels, the measured equivalent solids sizes are similar to each other at different air velocities and different mass flow rates, with small standard deviations. These results confirm that the integrated sensing approach yields repeatable measurements of solids size distribution.

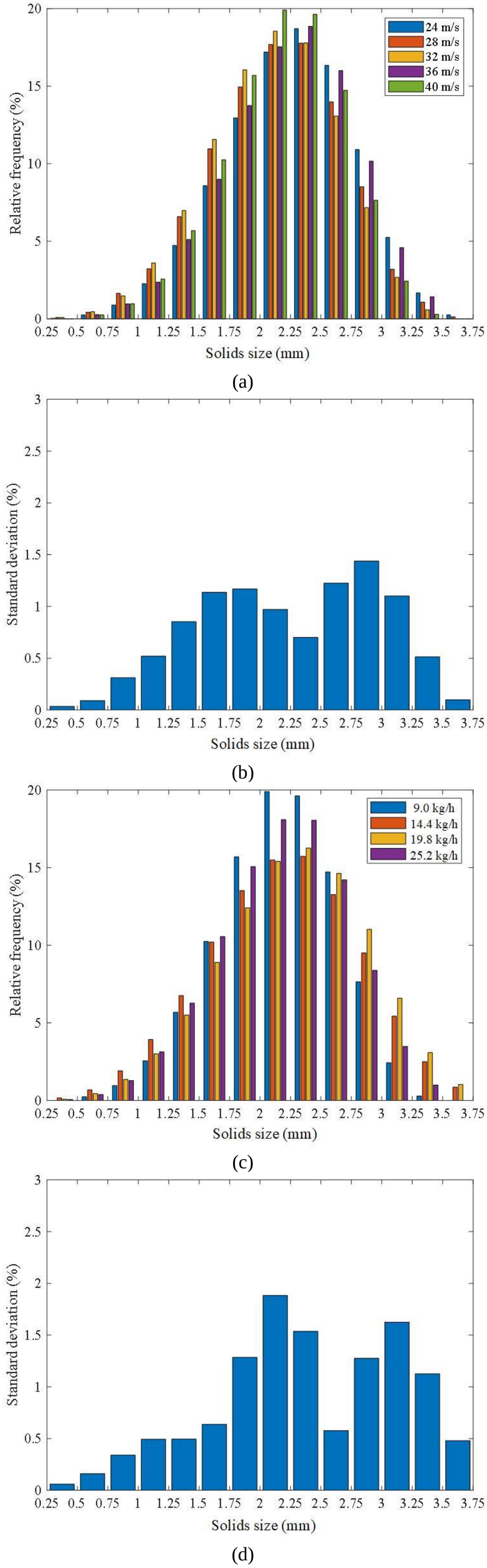

Fig.12. Measured size distribution of wheat straw. (a) Size distribution at different air velocities. (b) Standard deviations of the size distribution at different air velocities. (c) Size distribution at different mass flow rates. (d) Standard deviations of the size distribution at different mass flow rates.

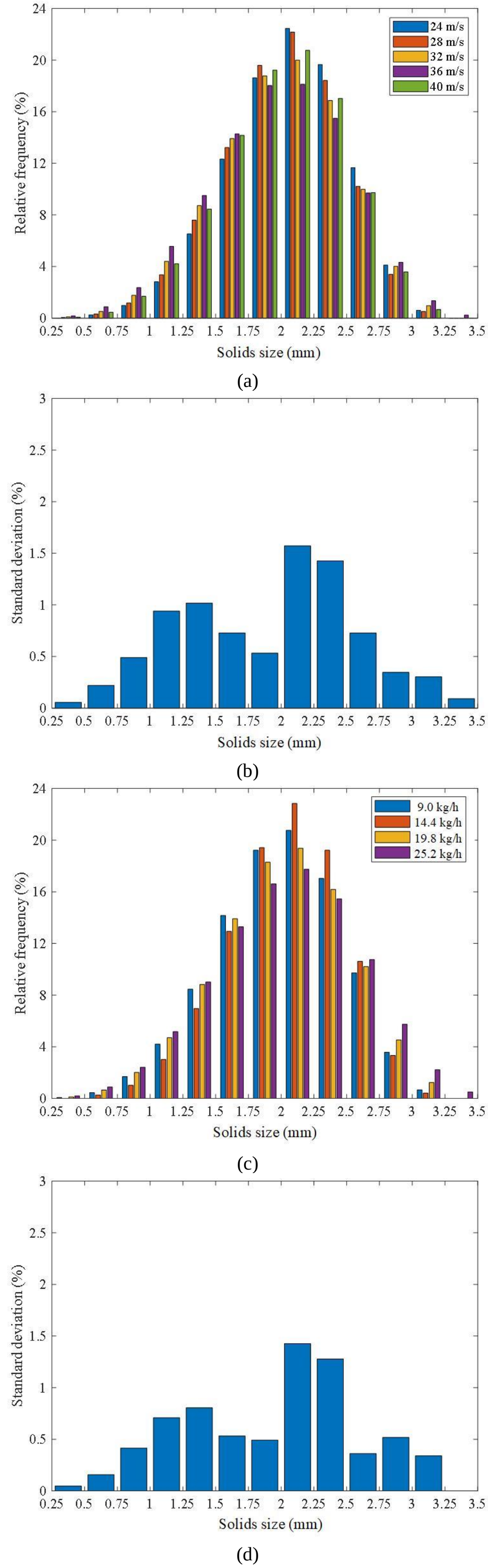

Fig.13. Measured size distribution of sawdust. (a) Size distribution at different air velocities. (b) Standard deviations of the size distribution at different air velocities. (c) Size distribution at different mass flow rates. (d) Standard deviations of the size distribution at different mass flow rates.

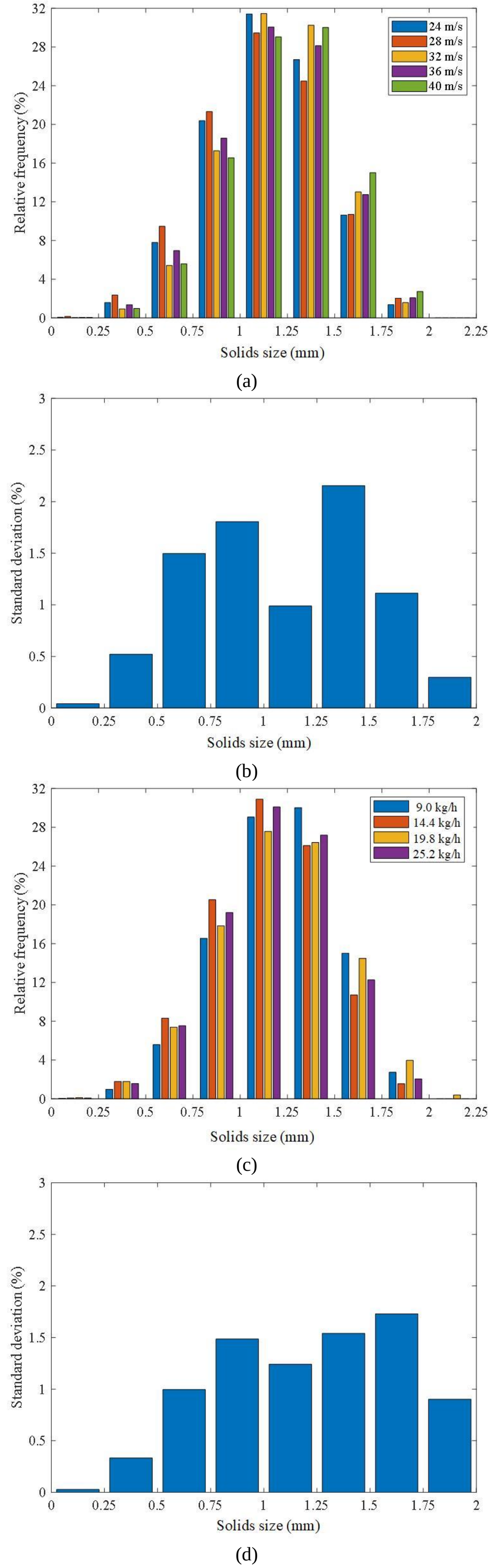

Fig.14. Measured size distribution of corncob. (a) Size distribution at different air velocities. (b) Standard deviations of the size distribution at different air velocities. (c) Size distribution at different mass flow rates. (d) Standard deviations of the size distribution at different mass flow rates.

The size measurement through AE detection is based on the impact theory, so the measured size is the equivalent impact diameter. By substituting the average size, length and length-width ratio of wheat straw, sawdust and corncob, which are obtained using the imaging equipment (Table I), into equation (7), we can determine the reference values of the average impact solids size as 2.20 mm, 1.92 mm and 1.18 mm, respectively. Fig. 15 shows the average values of the measured equivalent impact size under different test conditions in comparison with the reference values. Because of its highest irregularity wheat straw has the largest absolute error of the measured results with an overall relative error of within ±4.7%. The absolute error of the measured results of sawdust is less than that of wheat straw, but the worst relative error is ±6.45% because of the smaller reference solids size of sawdust. Due to its relatively regular shape, corncob has produced the smallest error of the measured results (±4.15%). The small measurement error stems both from the fluctuation of the measured equivalent impact size and from the natural variation in the biomass material during the test runs.

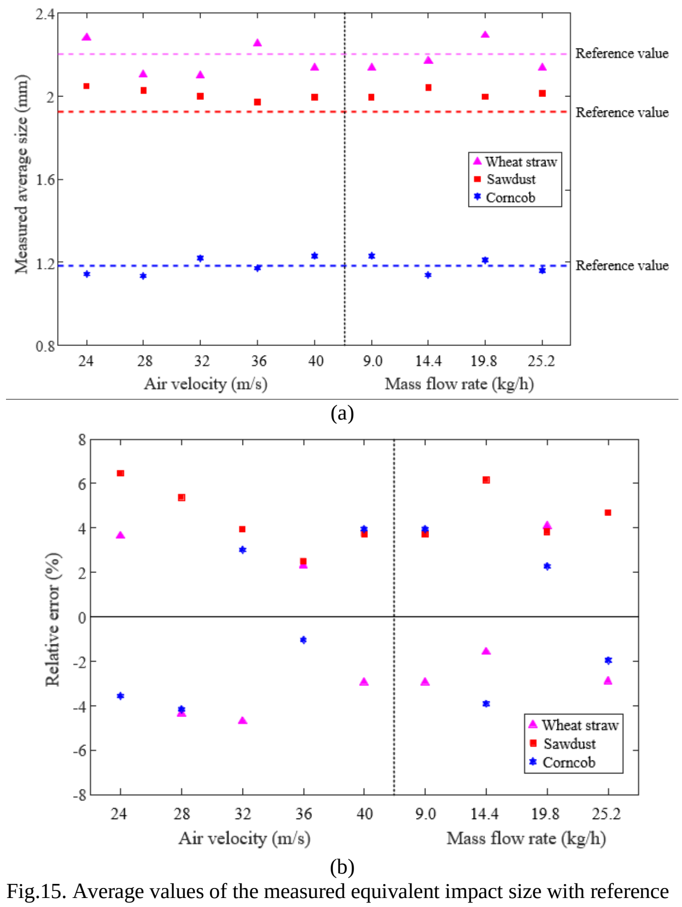

Fig.15. Average values of the measured equivalent impact size with reference to the imaging data. (a) Average values of equivalent impact size. (b) Relative error.

IV. CONCLUSION

A novel instrumentation system for the concurrent measurement of the size distribution and velocity of biomass fuels using AE and electrostatic sensors has been proposed. In view of the inelasticity and irregularity of biomass fuels, the inelastic impact theory based on the Stronge model has been applied. The relationship between the statistical value of equivalent impact size and the shape characteristics of irregular solids has been established. With the velocity information of biomass from the arc-shaped electrostatic sensor arrays, the measurement of the size distribution of biomass has been achieved. The experimental results have demonstrated that the pneumatic transportation of biomass fuels depends on such factors as solids shape and size. The size distribution measurement results have indicated that the standard deviation of the measured equivalent size distribution of biomass solids measured with a 30 s AE signal is less than 2.15% under all test conditions. With reference to the average solids size from the imaging method, the relative error of the measured average solids size is within ±6.45% for the three kinds of biomass. Future work will explore the performance of the developed technique for the size distribution measurement of mixed biomass and pulverized coal under co-firing conditions as well as crushed waste solids in waste incinerators.

Acknowledgment

Dr Ge Zheng and Professor Yong Yan would like to acknowledge the IEEE Instrumentation and Measurement Society for the 2021 Graduate Fellowship Award.

References

[1] C. Yin, “Development in biomass preparation for suspension firing towards higher biomass shares and better boiler performance and fuel range ability,” *Energy*, vol. 196, Art. no. 117129, 2020.

[2] S. A. Zaman and S. Ghosh, “Novel integration of molten carbonate fuel cell stacks in a biomass-based Rankine cycle power plant with CO2 separation: A techno-economic and environmental study,” *Energy*, vol. 307, Art. no. 132537, 2024.

[3] R. K. Pan, T. Qiu, J. K. Cha, H. Y. Ma, J. Wang and C. Li, “Thermal evolution of the oxidation characteristics of pulverized coal with different particle sizes and heating rates,” *Thermochim. Acta*., vol. 685, Art. no. 1785162, 2020.

[4] A. Malek A, M. Hasanuzzaman, N. Rahim and Y. Turki, “Techno-economic analysis and environmental impact assessment of a 10MW biomass-based power plant in Malaysia,” Journal of Cleaner Production, vol. 141, pp. 502-513, 2017.

[5] Y. Wang, X. Qian, L. Wang and Y. Yan, “Measurement of cross-sectional velocity distribution of pneumatically conveyed particles in a square-shaped pipe through gaussian process regression-assisted non-restrictive electrostatic sensing,” *IEEE Trans. Instrum. Meas.*, vol. 72, Art. no. 2504411, 2023.

[6] Y. Zheng and Q. Liu, “CFD simulation methodology for gas-solid flow in bypass pneumatic conveying – A review,” *Measurement*, vol. 44, no. 4, pp. 589-604, 2011.

[7] Y. Wang, K. Williams, M. Jones and B. Chen, “CFD simulation methodology for gas-solid flow in bypass pneumatic conveying – A review,” *Appl. Therm. Eng.*, vol. 125, pp. 185-208, 2019.

[8] O. Chit, K. Daisuke, O. Hiroyuki, T. Yuhi, Y. Yoshiyuki and T. Masahiro, “Particle volume flow rate measurement by combination of dual electrical capacitance tomography sensor and plug flow shape model,” *Powder Technol.*, vol. 364, pp. 310-320, 2020.

[9] A. Faisal, Y. Yan and L. Wang, “Mass flow rate measurement of pneumatically conveyed solids through multimodal sensing and data-driven modelling,” *IEEE Trans. Instrum. Meas.*, vol. 70, Art. no. 2513416, 2021.

[10] O. S. Alshahed, B. Kaur, M. S. A. Bradley and D. Chelu, “Application of nonlinear dynamics analysis to gas-solid flow system in horizontal pneumatic conveying of plastic pellets,” *Powder Technol.*, vol. 428, Art. no. 118837, 2023.

[11] Z. Zhu, Y. Wang, D. Wang, G. Yang and Z. Xie, “Evaluation of array capacitive sensor for local concentration measurement of gas–solid particles flow by coupled fields based on CFD-DEM,” *Measurement*, vol. 229, Art. no. 114457, 2024.

[12] X. Qian, Y. Yan, X. Huang and Y. Hu, “Measurement of the mass flow and velocity distributions of pulverized fuel in primary air pipes using electrostatic sensing techniques,” *IEEE Trans. Meas. Instrum.*, vol. 66, no. 5, pp. 944-952, 2017.

[13] H. Schneider, M. Bonarens, J. Hebel, H. Hamel, J. Emmert, B. Böhm, S. Wagner, R. Kneer and A. Dreizler, “Combined flow, temperature and soot investigation in oxy-fuel biomass combustion under varying oxygen concentrations using laser-optical diagnostics,” *Fuel*, vol 362, Art no 130771, 2024.

[14] D. Li, Q. Jing, Y. Wang and L. Guo, “The application of maximum entropy technique to determine number concentration and size distribution in pneumatic transport,” *Energy Rep.*, vol. 8, pp. 131-140, 2022.

[15] Q. Jin, L. Zeng, X. Chen, P. Li, H. Fu, Y. Zhou, Y. Wu and X. Wu, “Portable digital holographic particle analyzer (DHPA) for pneumatically conveyed fuel monitoring: Design and validation,” *Powder Technol.*, vol. 430, Art. no. 119030, 2023.

[16] L. Chen, H. Ma, G. Ma, Z. Sun and K. Gao, “Experimental investigation of pressure drop of spherical and non-spherical coarse particles in pneumatic conveying in horizontal pipes”, *Powder Technol.*, vol. 444, Art. no. 120031, 2024.

[17] J. Gu, M. Su and X. Cai, “In-line measurement of pulverized coal concentration and size in pneumatic pipelines using dual-frequency ultrasound”, *Appl. Acoust.*, vol. 138, pp. 163-170, 2018.

[18] S. Zhang, G. Su, H. Liu, C. Tian and M. Su, “On-line measurement of particle size in high-concentration limestone slurry pipeline by Monte-Carlo based ultrasonic attenuation model,” Measurement, vol. 235, Art. no. 115007, 2024.

[19] L. Jia, C. Wang, Y. Li and J. Ye, “Electrostatic charge distribution-based direct velocity tomography method for gas–solid two-phase flow,” *IEEE Trans. Instrum. Meas.*, vol. 70, Art. no. 4506812, 2021.

[20] C. Park, S. Chowdhury, Y. Pottimurthy, Q. Marashdeh and A. Tong, “Velocity profiling of a gas–solid fluidized bed using electrical vapacitance volume tomography,” vol. 77, Art. no. 4504516, 2022.

[21] A. Boschetto and F. Quadrini, “Powder size measurement by acoustic emission,” *Measurement*, vol. 44, no. 1, pp. 290-297, 2011.

[22] M. G. Droubi, R. L. Reuben and G. White, “Monitoring acoustic emission (AE) energy in slurry impingement using a new model for solid impact,” *Mech. Syst. Signal Proc.*, vol. 62-63, pp. 415-430, 2015.

[23] E. Hansuld, L. Briens and A. Sayani, “An investigation of the relationship between acoustic emissions and particle size,” *Powder Technol.*, vol. 219, pp. 111-117, 2012.

[24] P. J. Coghill, “Solid size of pneumatically conveyed powders measured using impact duration,” *Part. Part. Syst. Charact.*, vol. 24, pp. 464-469, 2007.

[25] G. Zheng, Y. Yan, Y. Hu and W. Zhang, “Online measurement of the size distribution of pneumatically conveyed particles through acoustic emission detection and triboelectric sensing,” *IEEE Trans. Instrum. Meas.*, vol. 70, Art. no. 9506717, 2021.

[26] L. Gao, Y. Yan, R. Carter, D. Sun, P. Lee and C. Xu, “On-line particle sizing of pneumatically conveyed biomass particles using piezoelectric sensors,” *Fuel*, vol. 113, pp. 810-816, 2013.

[27] Y. Yan, Y. Hu, L. Wang, X. Qian, W. Zhang, K. Reda, J. Wu and G. Zheng, “Electrostatic sensors – their principles and applications,” *Measurement*, vol. 169, Art. no. 108506, 2021.

[28] J. Coombes and Y. Yan, “Measurement of velocity and concentration profiles of pneumatically conveyed particles using an electrostatic sensing array,” *IEEE Trans. Instrum. Meas.*, vol. 65, pp. 1139-1148, 2016.

[29] X. Qian, Y. Yan, S. Wu and S. Zhang, “Measurement of velocity and concentration profiles of pneumatically conveyed particles in a square-shaped pipe using electrostatic sensor arrays,” *Powder Technol.*, vol. 377, pp. 693-708, 2021.

[30] Y. Hu, Y. Yan, X. Qian and W. Zhang, “A comparative study of induced and transferred charges for mass flow rate measurement of pneumatically conveyed particles,” *Powder Technol.*, vol. 356, pp. 715-725., 2019.

[31] F. Liu, J. Zhang and J. Chen, “Modeling of flexible wheat straw by discrete element method and its parameter calibration,” *Int. J. Agric. Biol. Eng.*, vol. 11, pp. 42-46, 2018.

[32] M. Stasiak, M. Molenda, M. Bańda and E. Gondek, “Mechanical properties of sawdust and woodchips,” *Fuel*, vol. 159, pp. 900-908, 2015.

[33] J. Stronge, *Impact Mechanics*. Cambridge, U.K.: Cambridge Univ. Press, 2004.

[34] J. Litster, *Design and processing of particulate products*. Cambridge, U.K.: Cambridge Univ. Press, 2016.

[35] Y. Kuahai and T. Danesh, “Impact model for micrometer-sized sand particles,” *Powder Technol.*, vol. 294, pp. 11-21, 2016.

[36] H. Merkus, *Particle size measurements: Fundamentals, practice, quality.* Dordrecht, Netherlands: Springer, 2009.

[37] P. Bowen, “Particle size distribution measurement from millimeters to nanometers and from rods to platelets,” *J. Dispersion Sci. Technol.*, vol. 23, pp. 631-662, 2002.

[38] M. Sommerfeld, “Kinetic simulations for analysing the wall collision process of non-spherical particles”, in *Proc. European Fluids Engineering Division Conference*, vol. 36169, pp. 539-547, 2002.

[39] Y. Hu, L. Wang, X. Huang X. Qian, L. Gao and Y. Yan, “On-line sizing of pneumatically conveyed solids through acoustic emission detection and signal analysis,” *IEEE Trans. Instrum. Meas.*, vol. 64, no. 5, pp.1100-1109, 2015.

[40] D. Malav, R. Ganguli, S. Dutta and S. Bandopadhyay, “Non-impact of particle size distribution on power generation at a pulverized coal power plant burning low rank Alaska coal,” *Fuel Process. Technol.*, vol. 89, no. 5, pp. 499-502, 2008.

[41] A. Macias-Garcia, E. Cuerda-Correa and M. Diaz-Diez, “Application of the Rosin-Rammler and Gates-Gaudin-Schuhmann models to the particle size distribution analysis of agglomerated cork,” *Mater. Charact.*, vol. 52, no. 2, pp. 159-164, 2004.

[42] R. Carter, Y. Yan and P. Lee, “On-line nonintrusive measurement of particle size distribution through digital imaging,” *IEEE Trans. Instrum. Meas.*, vol. 55, no. 6, pp. 2034-2038, 2006.

[43] S. Gubba, D. Lngham and K. Larsen, “Investigations of the transportation characteristics of biomass fuel particles in a horizontal pipeline through CFD modelling and experimental measurement,” *Biomass and Bioenergy*, vol. 46, pp. 492-510, 2012.